An Atomic Model of Actin Filaments Cross-linked by Fimbrin and Its Implications for Bundle Assembly and Function

Niels Volkmann,* David DeRosier,‡ Paul Matsudaira,§ and Dorit Hanein*

*The Burnham Institute, La Jolla, California 92037; ‡The Rosenstiel Basic Medical Sciences Research Center and The W.M. Keck Institute for Cellular Visualization, Brandeis University, Waltham, Massachusetts 02254; and §Whitehead Institute for Biomedical Research, Massachusetts Institute of Technology, Cambridge, Massachusetts 02142

Abstract. Actin bundles have profound effects on cellular shape, division, adhesion, motility, and signaling. Fimbrin belongs to a large family of actin-bundling proteins and is involved in the formation of tightly ordered cross-linked bundles in the brush border microvilli and in the stereocilia of inner ear hair cells. Polymorphism in these three-dimensional (3D) bundles has prevented the detailed structural characterization required for in-depth understanding of their morphogenesis and function. Here, we describe the structural characterization of two-dimensional arrays of actin cross-linked with human T-fimbrin. Structural information obtained by electron microscopy, x-ray crystallography, and homology modeling allowed us to build the first molecular model for the complete actin–fimbrin cross-link. The restriction of the arrays to two dimensions allowed us to deduce the spatial relationship between the components, the mode of fimbrin cross-linking, and the flexibility within the cross-link. The atomic model of the fimbrin cross-link, the cross-linking rules deduced from the arrays, and the hexagonal packing of actin bundles in situ were all combined to generate an atomic model for 3D actin–fimbrin bundles. Furthermore, the assembly of the actin–fimbrin arrays suggests coupling between actin polymerization, fimbrin binding, and crossbridge formation, presumably achieved by a feedback between conformational changes and changes in affinity.

Key words: calponin homology domain • electron microscopy • image analysis • homology modeling • two-dimensional arrays

Introduction

Cells organize their actin filaments into three-dimensional (3D)[1] bundles using a large repertoire of actin–cross-linking proteins (Ayscough, 1998; Puius et al., 1998; Bartles, 2000). Actin bundles support and stabilize cellular protrusions, invaginations, or domains of the plasma membrane and thus have profound effects on cellular shape, division, adhesion, motility, and signaling. The actin cross-linkers are conserved throughout the eukaryotic kingdom and found to have a modular organization (Matsudaira, 1991). They are composed of a pair of actin-binding domains (ABDs), variable spacer domains, and sometimes a regulatory domain. In one cross-linking class, the conserved ABDs consist of tandem pairs of calponin homology (CH) domains (Castresana and Saraste, 1995; Banuelos et al., 1998). Proteins containing tandem pairs of CH domains include α-actinin, dystrophin, fimbrin, spectrin, and utrophin. The simplest modular arrangement within the cross-linkers of this family is found in fimbrin, where two ABDs are arranged on the same polypeptide chain without any spacers, directing the formation of densely packed bundles. In the rest of the family, tandem organization of two ABDs is achieved through protein dimerization.

In vivo, fimbrin is involved in the formation of actin bundles in the microvilli of the brush border epithelia cells and in the hair cell stereocilia of the inner ear (Tilney et al., 1989, 1992). The tightly packed arrays of the microvilli amplify the apical surface of the absorptive epithelial cells, and the stereocilia serve as mechanosensory devices implicated in transduction of sound-induced motion. Fimbrin is the major actin-bundling protein of the hair cell stereocilia. Fimbrin and villin are the major cross-linkers of the microvilli core. However, ultrastructural studies of intestinal microvilli in villin-null mice indicate that villin is not a critical determinant for bundle assembly (Pinson et al., 1998; Ferrary et al., 1999). Microvilli as well as stereocilia bundles contain parallel actin filaments that share the same polarity and are packed in a hexagonal lattice with their filament barbed ends facing the cell surface (De-

Address correspondence to Dorit Hanein, The Burnham Institute, 10901 North Torrey Pines Rd., La Jolla, CA 92037. Tel.: (858) 646-3134. Fax: (858) 646-3196. E-mail: dorit@burnham.org

[1]*Abbreviations used in this paper:* 2D, two-dimensional; 3D, three-dimensional; ABD, actin-binding domain; ABD1, NH_2-terminal ABD of fimbrin; ABD2, COOH-terminal ABD of fimbrin; CH, calponin homology.

Rosier and Tilney, 1982; Tilney et al., 1983, 2000). The actin-bundling activity of fimbrin is inhibited by calcium (Namba et al., 1992; Lin et al., 1994).

Understanding the mechanism of bundle assembly and function requires detailed structural information. However, disorder and polymorphism limit the structural information that can be extracted from actin bundles directly. To constrain this polymorphism, here we restricted the cross-linking to two dimensions and analyzed the structural organization of actin and of actin arrays cross-linked with human T-fimbrin. In the cross-linked arrays we found two distinct types of cross-link conformations, leading to straight or slanted crossbands. The actin filaments in these arrays are unipolar, consistent with the organization observed in bundles in vivo (DeRosier and Tilney, 2000). In addition, the distance (~120 Å) between adjacent filaments in the fimbrin–cross-linked arrays agrees with the average distance reported for microvilli bundles (Matsudaira et al., 1983; Coluccio and Bretscher, 1989). The assembly of the two-dimensional (2D) actin–fimbrin arrays in our experimental setting suggests coupling between actin polymerization, fimbrin binding, and crossbridge formation.

The structural information derived from the arrays and the structure of an actin–fimbrin (ABD) complex (Hanein et al., 1998) were used to generate the first atomic model of complete actin–fimbrin cross-links. The model provides evidence for flexibility of the actin–fimbrin cross-link, that can be accommodated by the torsional freedom of actin filaments (Egelman and DeRosier, 1992; Orlova and Egelman, 2000) and rearrangements at the interface between the two ADBs of fimbrin. The observed flexibility of the cross-link, the resulting constraints on the cross-linking rules, and the hexagonal packing of actin bundles in situ (Tilney et al., 1983, DeRosier and Tilney, 2000) allowed us to build an atomic model for actin–fimbrin bundles. This model supports a mechanism for bundle bending through tilting of the crossbridges, consistent with the observations of bent stereocilia bundles in which the actin filaments slide past each other and do not stretch or compress (Tilney et al., 1983). In vivo, bending of the bundle occurs during stereocilia stimulation by sound and motion.

Materials and Methods

Protein Purification

β-Actin was purified by Dr. I. Correia (Whitehead Institute, Cambridge, MA) (Rozycki et al., 1991). The G-actin was flash frozen in liquid nitrogen and stored as 1-mg aliquots at −80°C. Before use, aliquots were thawed, dialyzed against G-actin buffer (2 mM Tris, pH 8.0, 0.2 mM $CaCl_2$, 0.2 mM ATP, and 1 mM DTT), and clarified at 7.0×10^4 rpm for 30 min in a Beckman-Coulter TLA-100 rotor.

Human T-fimbrin was expressed in BL21 bacterial cells grown in 2X YT/Amp media, concentrated by centrifugation, and lysed in a French press. The 3/7 ammonium sulfate precipitate from a 18k × *g* supernatant of the cell lysate was resuspended in column buffer (50 mM NaCl, 1 mM EDTA, 1 mM DTT, 1 mM NaN_3, and 10 mM Tris, pH 8.0) and chromatographed through an AcA34 gel filtration column. Fimbrin-containing fractions were pooled and loaded onto a DEAE Sepharose fast flow column equilibrated in column buffer. The column was developed with a 0–300 mM gradient of NaCl in column buffer, and the fimbrin-containing fractions were pooled and diluted to 50 mM NaCl in column buffer. The fimbrin-containing fractions were loaded onto an fast protein liquid chromatography Q-HR Sepharose column and eluted with a 0–500 mM NaCl gradient in 1 mM EDTA, 1 mM DTT, 10 mM Pipes, pH 7.0. The fimbrin fractions were pooled and concentrated in a Centricon concentrator. By SDS-PAGE, the protein was at least 95% pure.

2D Arrays

Arrays were grown (8–24 h) at 4°C on positively charged lipid layers consisting of a 3:7 wt/wt solution of dilaurylphosphatidylcholine (Avanti Polar Lipids, Inc.) and didodecyldimethylammonium bromide (DDDMA; Acros Organic) dissolved in chloroform (Taylor and Taylor, 1994). The lipid–surfactant mixture (0.5 μl drop containing 0.5 μg lipids) was layered over the polymerization buffer before the injection of G-actin (~0.5 μM) for producing the F-actin arrays. The polymerization buffer contained 20 mM PO_4, pH 6.5, 40 mM KCl, 1 mM $MgCl_2$, 1 mM ATP, and 0.2 mM EGTA. For producing the actin–fimbrin arrays, the lipid–surfactant mixture was layered over the polymerization buffer containing fimbrin (~1 μM) before the injection of G-actin (~0.5 μM).

Electron Microscopy

Specimens were transferred to 400-mesh copper grids coated with holey carbon films (Kubalek et al., 1991). Specimens were washed with polymerization buffer before staining using 2% aqueous uranyl acetate and air dried. The samples stained and not washed had 3D bundles intersecting the 2D arrays. Specimens were examined on a CM12 electron microscope (FEI) under low-dose conditions. Low-dose images were recorded using 120 keV, at a nominal magnification of 60,000× and ~0.5-μm defocus (electron dose ~10 $e^- Å^{-2}$).

Image Processing

Images were scanned at a raster of 7 μm $pixel^{-1}$ using a SCAI scanner and an O2 workstation (SGI). 40 arrays of actin–fimbrin and 20 of fimbrin-free actin were chosen for image processing. The arrays were selected, boxed, and displayed with a modified version of Ximdisp (Smith, 1999). Fourier transforms were calculated using the Brandeis helical imaging package (Owen et al., 1996). All measurements (e.g., tilt and distance) relating to row-line offsets to determine rotational and translational relationships between neighboring filaments were done relative to the direction of the layer lines. This ensures that no bias is introduced by misalignment of the arrays in respect to the image coordinate system. Fourier filtering was done using the 2D crystallography software in the MRC image-processing package (Crowther et al., 1996).

Homology Modeling

Homology modeling was achieved using the program MODELLER4 (Sali and Blundell, 1993). We used the crystal structures of the fimbrin (PDB code 1AOA) and utrophin (1QAG) NH_2-terminal ABDI , and of the CH domain of β-spectrin (1AA2) for the modeling of the COOH-terminal ABD of fimbrin (ABD2). We used 48 EF-hand structures to model the NH_2-terminal calcium-binding domain.

Sequence Similarity

The sequence similarity between the residues of ABD1 and ABD2 was evaluated using a scoring matrix (PAM250, as used in FASTA; Pearson, 1990). The numbers in the scoring matrix are derived from the probability of substitution. The higher this number, the higher the sequence similarity. 68 residues were assigned as prospective interface residues using interaction probabilities for ABD1 (Hanein et al., 1998). The residues in ABD1 and ABD2 that were assigned to interact were identical in 29.4% of the cases; the ones in the remaining set were identical in 23.2% of the cases. The average similarity score for the interface residues was 2.265, and that for the remainder was 0.584. A *t* test reveals that this difference is statistically significant at a confidence level of 99.5% (p-value < 0.005).

Results

2D Arrays of Actin Filaments Cross-linked with Human T-Fimbrin

We polymerized G-actin on positively charged lipid surfaces (Ward et al., 1990; Taylor and Taylor, 1994) in the absence (Fig. 1 A) and in the presence (Fig. 1, B–C) of hu-

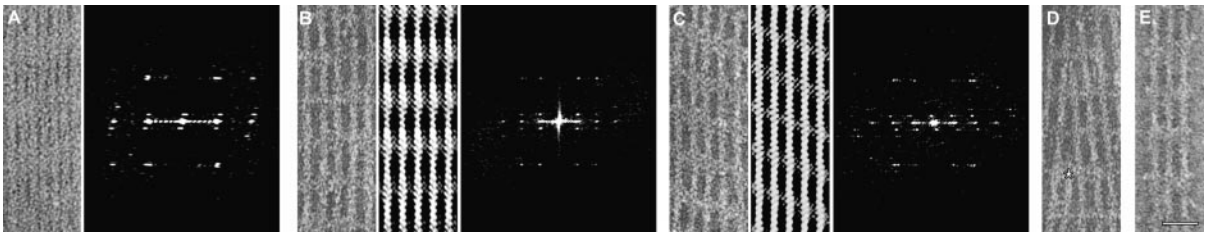

Figure 1. 2D arrays of actin and actin cross-linked with human T-fimbrin. (A) 2D array of fimbrin-free actin filaments and its Fourier transform. The tilt in the row lines indicates a counter clockwise rotation of 30°–40° between adjacent filaments. Note the somewhat weaker reflections in between the main row lines. The existence of these reflections indicates a bipolar organization of the filaments within the array. The resolution of the diffraction pattern is ~35 Å. (B–C) 2D arrays of actin cross-linked with fimbrin. Note the regular distance between the crossbridges. Only two types of crossband patterns are observed: straight (B) and slanted (C). (B) 2D array of actin–fimbrin array with straight crossband patterns, the Fourier-filtered image, and the Fourier transform of the array. Note that there is no tilt in the Fourier transform pattern, indicating that the filaments in the array are in register. Only contributions close to the diffraction spots were used to calculate the Fourier-filtered image of the straight crossband pattern seen in B. The crossband pattern in this fimbrin–cross-linked array appears slanted. Note the tilt of the Fourier pattern, corresponding to a clockwise rotation between adjacent filaments of ~27°. Due to actin's helical symmetry this is equivalent to a translation of 55 Å parallel to the helix axis. The resolution of the diffraction patterns in B and C is ~35 Å. (D) The figure shows the cross-linking behavior in a region where one filament terminates in the middle of a fimbrin cross-linked array (*). The two neighboring filaments can further cross-link the array with no disruption or alteration in the orientation of the newly formed crossbridges (at top of image), indicating that the three filaments shared the same polarity. (E) Small 2D array of actin cross-linked with fimbrin that shows side decoration. The abundance of fimbrin side decoration in both edges of cross-linked arrays, compared with rare decoration of single actin filaments in our experimental setting, supports the hypothesis that the presence of the actin-bound fimbrin molecule increases the affinity of the opposite F-actin–binding site on the same filament (Fig. 5 B, yellow), thus increasing the probability of binding a second fimbrin molecule at this site (Fig. 5). Bar, 25 nm.

man T-fimbrin. In the cross-linked arrays the crossbridges appear as regularly spaced bands either perpendicular or slanted relative to the axis of the actin filaments. Washing the preformed actin arrays with fimbrin resulted in sparse formation of cross-links and an appearance with no regular crossbands. A stoichiometry of one crossbridge per crossover (about every 13.5 actin monomers, 375 Å apart) is measured in gels (data not shown) as well as directly from the images.

Polarity and Spatial Relationships between Neighboring Filaments in the Fimbrin-free 2D Arrays. The filament arrays of actin in the absence of fimbrin are tightly packed and give rise to well-ordered computed diffraction patterns (Fig. 1 A). These patterns consist of spots lying on a series of horizontal lines called layer lines. These layer lines arise from the helical symmetry of the actin filaments (Fig. 2 A). Single filaments give rise to continuous layer lines. The sampling of the layer lines, at intersections with so-called row lines, is due to the paracrystalline order of the filaments (Fig. 2, A and B). The way the layer lines are sampled (tilt and distance of the row lines) gives information on the spatial relationship between neighboring filaments, i.e., orientation, the relative rotation, and axial shift (Sukow and DeRosier, 1998). The actin and actin–fimbrin arrays are highly ordered, as can be assessed from the clear visibility of individual F-actin monomers in the Fourier-filtered images and the resolution of diffraction patterns of individual arrays (Fig. 1, B and C, ~35 Å). This resolution is clearly sufficient to unambiguously determine the tilt and the distance of the row lines and thus the spatial relationship between neighboring filaments. Within the 20 fimbrin-free arrays analyzed, the interfilament distance between successive actin filaments is ~75–80 Å. The diameter of actin filaments in projection is ~90 Å. The fact that the interfilament distance is smaller than the projection diameter means that the packing must be extremely tight with relatively close contact distances between actin monomers of adjacent filaments. Within the actin arrays, we observe both unipolar and bipolar organization of adjacent filaments, with some preference to unipolar. We detect bipolar arrays by the occurrence of diffraction spots on the layer lines halfway in between the spots for unipolar arrays (Fig. 1 A). This additional sampling in the bipolar arrays results from the reduced symmetry generated by neighboring filaments having their polarities reversed (Sukow and DeRosier, 1998). The tilting of the row lines in the diffraction pattern indicates that adjacent actin filaments are rotated counter clockwise by 30–40°.

Polarity and Spatial Relationships between Neighboring Filaments in the Cross-linked 2D Arrays. In the fimbrin cross-linked arrays (Fig. 1, B and C), the spacing between the filaments as measured in real and reciprocal space is 115–120 Å, consistent with the distance of 120 Å measured by solution x-ray scattering from microvilli bundles (Matsudaira et al., 1983). This interfilament distance is also consistent with the distance predicted by the atomic model of the actin–fimbrin ABD complex (Hanein et al., 1998). In contrast, the interfilament distance of 2D actin arrays cross-linked with α-actinin, which is found in actin gels and networks, is ~390 Å (Taylor et al., 2000).

Contrary to the fimbrin-free actin arrays, the actin arrays cross-linked by fimbrin are always unipolar. Two lines of evidence support this unipolar organization of the filaments. First, inspection of the computed diffraction patterns of 40 cross-linked arrays shows that all layer lines are separated by a distance equal to the interfilament spacing (Fig. 1, B and C). No spots appear halfway in between. Second, where a filament ends within an array, the two neighboring filaments are cross-linked with no disruption to the array or alteration in the orientation of the crossbridges (Fig. 1 D). This indicates that the spatial relationship between the filament that ends and its two neighboring fila-

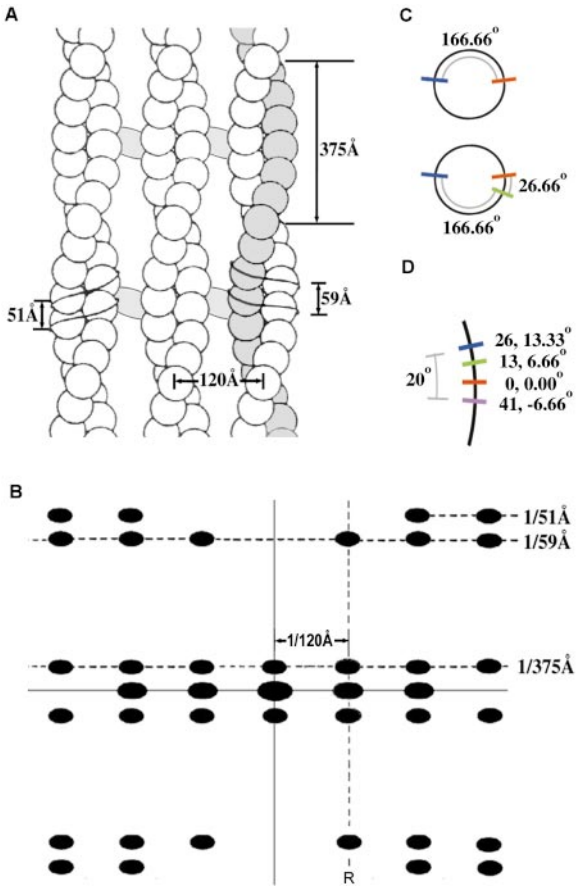

Figure 2. Schematic presentation for the symmetry and diffraction of cross-linked 2D actin arrays with crossover points in register. (A) Cross-linked actin array. The prominent helical families with pitches of 375, 59, and 51 Å are indicated. The cross-linker is shown in light gray, and the distance between the filaments is 120 Å. (B) Expected diffraction pattern of the array in A. The pattern consists of a series of horizontal lines that arise from the helical symmetry of actin. These layer lines occur at spacing of 1/375 Å, 1/59 Å, and 1/51 Å. The strong spots on the different layers are lined up in columns called row lines (R). The row lines arise from the paracrystalline order of the adjacent filaments. A rotation of the filaments with respect to their neighbors would cause a tilt of the row lines. Reversal of polarity between adjacent filaments would generate an additional sampling on the layer lines creating additional row lines halfway in between. (C) Schematic for the helical symmetry of actin filaments. The helical symmetry of the filament generates symmetry-equivalent actin monomers by a 166.66° rotation and a 27.5-Å translation along the filament axis. A schematic projection of an actin filament (top, circle) is shown. The blue binding site is generated by one symmetry operation (166.66° rotation and 27.5-Å translation from the red binding site). (The 27.5-Å translation is not seen in projection.) An additional binding site (green) generated by one additional symmetry operation from the blue binding site is also shown. Note that the red and green binding sites are two symmetry operations apart, leading to a 26.66° angular and a 55-Å translational offset (i.e., twice 166.66° is 333.33°, 26.66° short of 360° for the angular offset and twice 27.5 Å for the translational offset). By turning the filament 26.66° (as is the case of the slanted array in Fig. 1 C), the green binding site points exactly in the same direction as the red one, only 55 Å translated along the filament axis. (D) Rotational deviations of potential binding sites within an actin helix. The symmetry of the actin helix generates an exact rotational match after four crossovers or every 54 symmetry operations (13.5 monomers per crossover). The minimum possible angular offsets for generating one binding site per crossover (as is observed) is depicted here. The first binding site at actin monomer 0 is shown in red. The first crossover of the filament is 13.5 monomers from this starting position. The 13th monomer is 6.66° offset (green) from the starting position. The second crossover occurs after 27 monomers. This monomer is exactly 180° offset, corresponding to a reversal of the crossbridge direction. Although this possibility may occur in the straight crossbridge conformation, reversal of the direction cannot occur in the slanted conformation. Therefore, the crossbridge must bind either at the 26th (blue) or 28th monomer, both 13.3° off the starting position but in different directions. The third crossover occurs after 40.5 monomers. Without direction reversal, monomer 41 gives the smallest deviation with −6.66° (purple). The 54th monomer at the fourth crossover has the same geometry as the starting position. In total, a complete offset of 20° within three crossovers needs to be accommodated if direction reversal is not permitted. If direction reversal is permitted, a total offset of only 6.66° is required. Note that actin filaments display a 5°–6° root-mean-square random change in twist per monomer, indicating a flexibility that could help to accommodate the required offsets.

ments is identical to the spatial relationship between the two neighboring filaments. This is only possible if the polarity of the three filaments is the same. In vivo, microvilli and stereocilia actin–fimbrin bundles have also been shown to have unidirectional polarity (Tilney et al., 1980).

Crossbridge Conformations and Flexibility. We observed two types of crossbridge conformations, one producing straight crossbands (Fig. 1 B), the other producing slanted crossbands (Fig. 1 C). Only these two types of conformations exist, and both conformations can be easily identified by eye. We did not observe mixed arrays. Both arrays are distinct from actin arrays in the absence of fimbrin (Fig. 1 A). The slanted arrays display handedness and are always slanted in the same direction as shown in Fig. 1 C. The handedness in the slanted arrays indicates a preference of one side of the array for the lipid surface. As a consequence of their helical symmetry, actin filaments appear the same from all directions. Therefore, the preference of one side of the array for the lipid must result from the spatial relationship between the interfilament cross-link and the lipid. Handedness in arrays with straight crossband appearance, if it exists, cannot be assessed visually.

The diffraction patterns of the straight crossband conformation indicate that adjacent actin filaments are in register (Fig. 1 B). The rotation angle between adjacent filaments in the array can be deduced from the analysis of their corresponding diffraction patterns (Sukow and DeRosier, 1998). For the analyzed straight crossband arrays, these angles ranged beteen to −5° and +5° with a mean value close to zero. The diffraction patterns of the slanted crossbridge conformation indicate a clockwise rotation of ~27° between adjacent filaments (Fig. 1 C). The angles for all slanted arrays investigated fell into the range between 22° and 32°. Due to the helical symmetry of actin, a 26.66° rotation is equivalent to a translation of 55 Å towards its barbed end (Fig. 2 C). Thus, a transformation from the spatial relationship between adjacent filaments in the straight crossband array (in register) to the spatial relationship in the slanted crossband arrays can be simply achieved by sliding the neighboring filament down by

55 Å. If a cross-link in the straight crossband array is rotated by 180° and is bound to the same actin units on one filament, the free binding site of the cross-linker, due to fimbrin's geometry (Fig. 3), faces now in the same direction as before (towards the second filament), only transitionally shifted downwards by 55 Å. Thus, a similar cross-linker conformation can accommodate both crossband patterns if the cross-linker is rotated by 180° around its center of mass, and the roles of ABD1 and ABD2 are exchanged.

Can Fimbrin's ADBs Exchange Roles? Structural studies of F-actin complexes of α-actinin (McGough et al., 1994), fimbrin (ABD1) (Hanein et al., 1997), and utrophin (Moores et al., 2000) have all suggested that the conserved ABDs of this cross-linker superfamily (Matsudaira, 1994; Castresana and Saraste, 1995) bind a similar surface on actin. Results of peptide deletion studies and suppressor mutant analysis for fimbrin and several other members of the superfamily also indicate that the ABDs of this family bind a similar surface on actin (Mimura and Asano, 1987; Lebart et al., 1990; Bresnick et al., 1991; Levine et al., 1992; Fabbrizio et al., 1993; Corrado et al., 1994; Holtzman et al., 1994; Honts et al., 1994; Brower et al., 1995). Sequence similarity between fimbrin residues proposed to interact with actin (Fig. 4, A and B) is significantly higher (p-value < 0.005) than the similarity between residues not involved in actin binding, further supporting the notion that the roles of ABD1 and ABD2 can be exchanged. However, despite the high sequence similarity, there is relatively low sequence identity (29.4%) in the residues involved in actin binding, indicating that ABD1 and ABD2 may generate non-identical interactions with actin. This is consistent with the identification of two separate dissociation constants for plant fimbrin from *Arabidopsis thaliana*, presumably one for each ABD (Kovar et al., 2000), and results obtained by suppressor mutant studies of yeast fimbrin. A tryptophan residue that is absolutely conserved in all ABDs of the su-

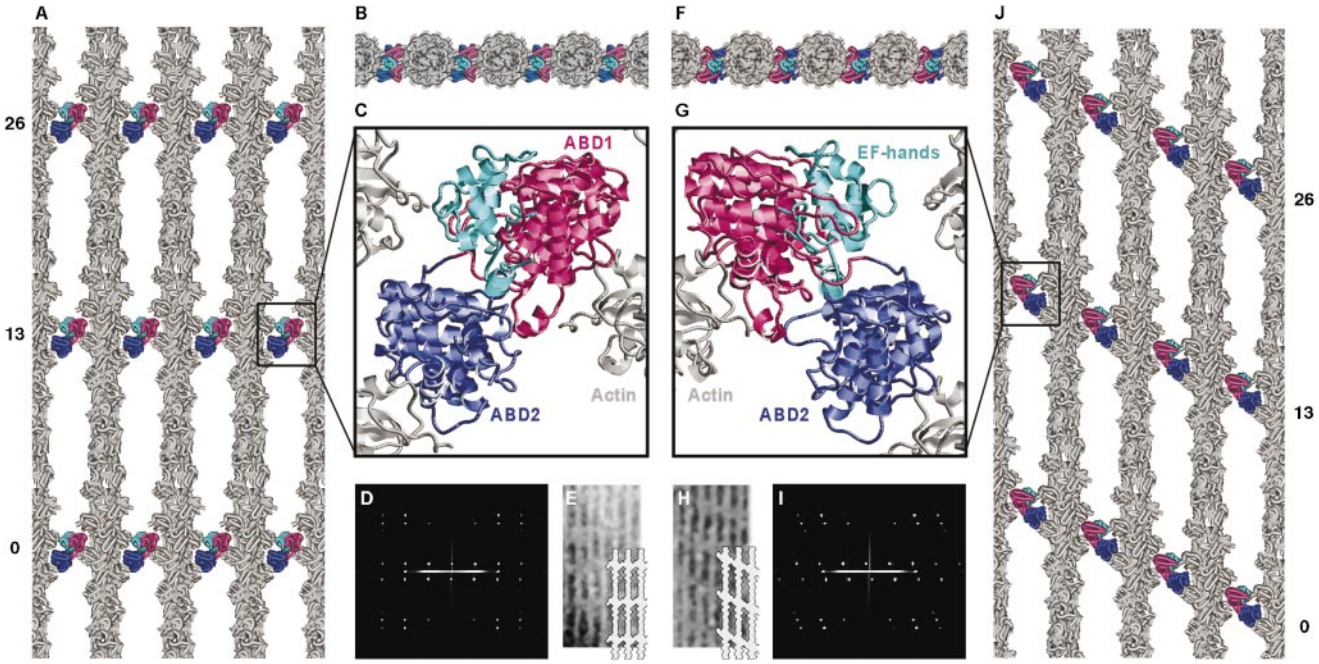

Figure 3. Atomic models of 2D actin arrays cross-linked by fimbrin. The spatial relationships between the filaments for the two types of arrays were deduced from the observed diffraction patterns (Fig. 1, B and C). The filaments in the micrographs with straight crossbands are in register. The filaments in the micrographs with slanted crossbands are rotated by 26.66° in respect to their neighbors. This operation exposes the same actin interface only one notch down (also Fig. 2 C and its corresponding legend). (A–C) Model of the straight crossband with filaments in register. Actin is shown in gray, ABD1 in pink, ABD2 in blue, and the NH_2-terminal calcium-binding domain (EF-hands) in cyan. The spatial relationship between the filaments and the ABDs was taken from the atomic model of actin–ABD1 (Hanein et al., 1998). The position of the calcium-binding domain was deduced from the difference peak between the docked model and the observed 3D reconstruction (solid red peak in Figure 3 of Hanein et al., 1998). ABD2 and ABD1 could be exchanged in principle; however, steric clashes between ABD2 and the calcium-binding domain would result if we exchange the ABD1 with ABD2. (A) Shows a side view of the arrays (as seen by the microscope). The actin monomers are enumerated, crossbridges occur at positions 0, 13, and 26 (as in Fig. 2 D). (B) Shows a view looking down the filament axes. The lipid layer is located on top of the figure. (C) A magnified view of a cross-link. (D) Fourier transform of the 2D array in A. Note how well the pattern matches Fig. 1 B. (E) Overlay of an enhanced version of an observed micrograph and a scaled version (light gray) of the atomic model in A. Note how well the crossband and filament distances correspond. (F–G and J) Model of the slanted crossband with adjacent filaments rotated by 26.66°, equivalent to a 55-Å downward translation. This geometry can be achieved by rotating fimbrin by 180° around its center of mass parallel to the filament axes and accommodating for the slight offset of fimbrin's geometry from exact rotational geometry. This symmetry is immediately evident by comparing B and F. Note the seemingly different position of the calcium-binding domain (C and G) is due to slightly different views. (F) A view looking down the filaments. The lipid layer is located on top of the figure. The criterion for handedness in this arrangement would be a preference for maximum distance from the lipid layer. (J) A side view, and (G) a magnified view of a cross-link. (H) Overlay of an enhanced version of an observed micrograph and a scaled version (light gray) of the atomic model in J. Note how well the crossband and filament distances correspond. (I) Fourier transform of the 2D array in J. Note how well the pattern matches Fig. 1 C.

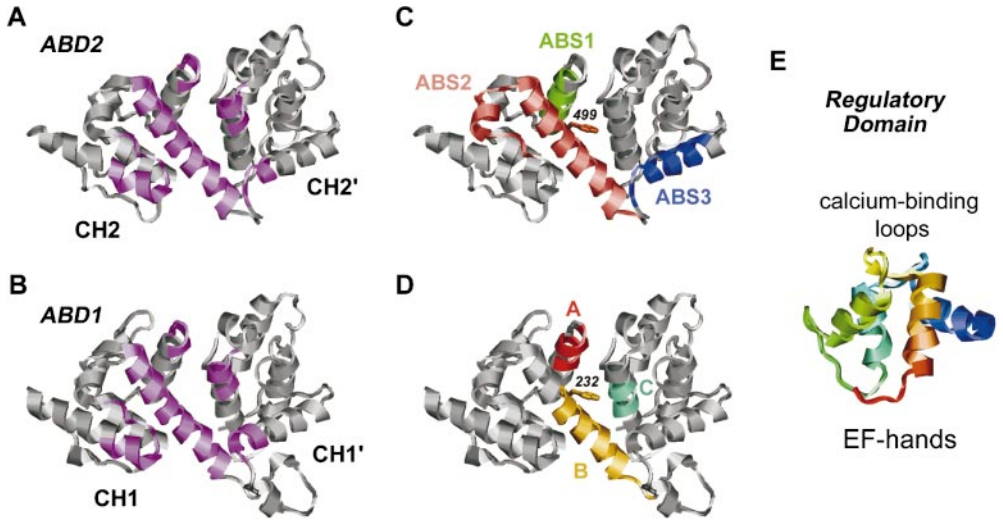

Figure 4. Atomic models and proposed actin-binding residues. (A) Homology-derived atomic model of ABD2. The residues proposed to participate in actin-binding according to the actin-N375 (ABD1) atomic model (Hanein et al., 1998) are mapped onto the model (magenta). Each of fimbrin ABDs contains two CH domains (CH1 and CH1′, and CH2 and CH2′, respectively). The two CH domains of ABD2 are labeled CH2 (NH_2-terminal) and CH2′ (COOH-terminal). (B) Atomic model of ABD1 (Goldsmith et al., 1997). The residues proposed to participate in actin binding according to the actin-N375 (ABD1) atomic model (Hanein et al., 1998) are mapped in magenta. (C) The residues homologous to the three actin-binding segments (ABS1-3) previously indicated as actin-binding sites by peptide deletion studies (Levine et al., 1992; Bresnick et al., 1991) mapped onto the ABD2 model. The ABSs are color coded: ABS1, green; ABS2, salmon; and ABS3, blue. Note the overlap of the proposed binding sites in A and B with ABS1-3. (D) The three clusters of mutations (A, red; B, yellow; C, light green) involved in actin binding identified by suppressor mutant analysis (Brower et al., 1995) mapped onto ABD1. Note the overlap of the proposed binding sites in A and B with these clusters. A tryptophan residue in cluster B is absolutely conserved in all ABDs of the superfamily (residue 232 in ABD1 and residue 499 in ABD2, human T-fimbrin sequence, both shown in stick representation). These residues are also part of ABS2 and the predicted interface of the actin-N375 model. Equivalent mutations (W232C and W499C) of the tryptophan in ABD1 and ABD2 in yeast showed different levels of suppression, suggesting nonidentical interactions of the ABDs with actin (Brower et al., 1995). (E) The atomic model of the EF-hands of the regulatory NH_2-terminal calcium-binding domain of fimbrin. The model was derived by sequence homology. Color coded, blue to red, from the NH_2 to COOH terminus.

perfamily show different levels of suppression for equivalent mutations in ABD1 (W252C, human T-fimbrin sequence) and ABD2 (W499C, human T-fimbrin sequence) (Fig. 4, C and D) (Brower et al., 1995).

As a consequence of the filament symmetry (~2.16 actin monomers per turn, 27.5 Å rise per monomer), the exact spatial relationship needed for the formation of the crossbridge only occurs every fourth crossover (every 54 monomers). The three crossovers in between are offset from this spatial relationship (Fig. 2 D, and its respective legend). The observed crossband patterns and the biochemical analysis indicate one crossbridge per crossover. How can this be accomplished? The straight crossbridge formation can be achieved with an angular deviation of only 6.66° by allowing direction reversal of the crossbridges every 27 monomers. The slanted crossband conformation needs deviations up to 20° since it cannot be built with reversal of the crossbridge direction due to its handedness. The existence of the slanted crossbridge conformation therefore necessitates that the actin cross-linker complex can be deformed to accommodate a ≤20° difference over four crossovers. However, the flexibility of the actin cross-linker system must be <26.66°, otherwise the cross-linker can accommodate both crossband patterns within the same array, i.e., a slanted crossband pattern in arrays with filaments in register. The later type of crossband pattern is not observed experimentally. The torsional freedom in actin, which expresses itself in a 5°–6° root-mean-square random change in the twist per monomer (Egelman and DeRosier, 1992; Orlova and Egelman, 2000), is likely to be a contributor to the actin cross-linker flexibility that allows the binding at the offset monomers. The variable twist of the actin filaments together with the flexibility of fimbrin give enough freedom to accommodate the observed range of crossbridge conformations while maintaining specific actin–fimbrin interactions. Crystal structures of the ABDs of several members of the superfamily have shown different dimer arrangements (Keep et al., 1999, Norwood et al., 2000), suggesting that the flexibility of fimbrin can be achieved through rearrangements of the ABD1-ABD2 interface.

Actin–Fimbrin Cross-link

We provided measurement of stoichiometry of fimbrin in 2D arrays (one crossbridge per crossover), the polarity (unipolar) and the spacing between adjacent cross-linked filaments (115-120 Å), the conformations of the crossbridge, and flexibility of the actin–fimbrin cross-link. We used this information to deduce the spatial relationships between the components of the cross-link. The knowledge of the spatial relationships allows us to build a model of the 2D arrays by putting the components together in a way that satisfies these relationships. To build the atomic model of an interfilament cross-link, we also need atomic models for the components. The crystal structure of the NH_2-terminal ABD1 of fimbrin (Goldsmith et al., 1997), as well as an atomic model of the actin-ABD1 complex (Hanein et al., 1998), is available. The atomic structures of the ABD2 and the NH_2-terminal regulatory domain of fimbrin are still not known. Therefore in this study, we generated models of both domains through the use of homology modeling (Sali and Blundell, 1993).

Homology Modeling of the NH_2-terminal Calcium-binding Domain. Sequence analysis shows that there are two tentative EF-hand motifs in the NH_2-terminal regulatory cal-

cium-binding domain of fimbrin (de Arruda et al., 1990). There are currently more than 90 EF-hand structures in the Protein Data Bank. 48 of these have sequence identity larger than 37.5%. Using these structures as the basis for the homology modeling, we obtained an atomic model of the domain (Fig. 4 E). Although the secondary structure of the NH_2-terminal domain is well defined by the high homology with other EF-hand motifs, the exact spatial arrangement of these structural elements remains uncertain. The relative orientation between the helices of the EF-hand motifs is known to be flexible (Yap et al., 1999). We initially modeled the relative orientation according to troponin C, the structure with the highest sequence identity (47.9%), and refined it later using spatial constraints from the rest of the structural domains of the model.

Homology Modeling of ABD2. We modeled the two CH domains that make up ABD2 independently. We used CH domains from the crystal structures of the fimbrin ABD1 (Goldsmith et al., 1997), utrophin ABD1 (Keep et al., 1999), and the CH domain of β-spectrin (Carugo et al., 1997), making a total of five known CH domain structures. ABD1 of fimbrin was used as a scaffold for the relative conformation of the two CH domains of ABD2 (Fig. 4 A). The decision to use fimbrin's ABD1 as a scaffold rather than utrophin's ABD1 was guided by the observations that ABD1 and ABD2 share a similar binding site on actin (Holtzman et al., 1994; Honts et al., 1994; Brower et al., 1995). This can only be achieved if ABD2 is in a fimbrin-ABD1–like conformation.

Building a Cross-link. Spatial Relationship between ABD1, ABD2, and the Calcium-binding Domain. The spatial relationship between ABD1 and the calcium-binding domain was provided through the fitting of ADB1 crystal structure into helical reconstructions of actin decorated with N375 (fimbrin ABD1 plus calcium-binding domain) (Hanein et al., 1998). A prominent peak, calculated from the difference between the observed density and the docked atomic model, localized the calcium-binding domain at the interface between the CH domains of ABD1 on the side facing away from the actin filament. This spatial arrangement places constraints on the relative orientation of the EF-hand helices, narrowing the possibilities down to a small number of relative arrangements. We selected one arrangement that fulfills these spatial constraints and also places both Ca^{++} binding sites exposed to solvent. The spatial relationship between the actin filaments and ABD1 as well as the actin-ABD1 residues involved in binding have been also establish (Hanein et al., 1998). The distance between filaments in the 2D arrays helps to define the distance between the ABDs. There are two ways in which to add ABD2 and a second actin filament to form a complete interfilament cross-link. One arrangement leads to clashes between ABD2 and the calcium-binding domain, but the other one does not. Our model in Fig. 3 corresponds to the model without clashes. We cannot deduce from the data whether the handedness of the slanted crossband conformation is due to a preferred distance or a preferred orientation of the crossbridges relative to the lipid layer. The arrangement in Fig. 3 shows a similar relative distance of the crossbridges from the lipid interface in the straight crossband conformation and the slanted conformation (Fig. 3, B and F). The distance is the more likely cause for handedness, since we do not observe excess fimbrin bound to the lipid. However, a similar relative orientation, i.e., exposing the same surface patch of fimbrin to the lipid, can be achieved by simply flipping the straight array in Fig. 3 by 180° parallel to the actin filament axis (around the paper plane), without altering the crossbridge model or the relative orientations between actin and the crossbridges. Our model is fully compatible with the observed diffraction patterns (compare the patterns calculated from the model in Fig. 3, D and I, with the observed ones in Fig. 1, B and C) as well as with the real space images of the 2D arrays (Fig. 3, E and H).

Discussion

2D Assembly Mechanism

Fimbrin imposes a regularity on the cross-linked array that is different from that observed in fimbrin-free actin arrays. It is interesting to note that fimbrin does not incorporate well into preformed actin arrays. We observed only a partial formation of cross-links and no regular crossbands in this case (data not shown). The regular appearance of the crossbands within the arrays (slanted or straight) indicates that the binding of fimbrin to actin occurs only at very specific binding sites and not in a random manner. The observation that regular crossbands only form when filaments are polymerized in the presence of fimbrin suggests that array formation requires coupling between actin polymerization and cross-link assembly. This notion is supported by the fact that in vitro yeast fimbrin (Sac6p) restores polymerization and bundle formation of a polymerization-defective yeast actin (GG-actin) (Cheng et al., 1999). Sac6p is also required for cell viability in the GG-actin phenotype in vivo (Cheng et al., 1999). In addition, the sedimentation behavior of F-actin from *A. thaliana* in the presence and absence of fimbrin suggests that fimbrin may promote actin polymerization and is capable of cross-linking very short segments of actin filaments (Kovar et al., 2000).

How can specific binding of fimbrin generate the observed crossband patterns? One possibility is that either fimbrin or actin (or both) sense the presence of a bound molecule at the opposite side of the actin filament. It is known that ABD1 binding initiates conformational changes within F-actin (Hanein et al., 1997), providing a possible mechanism for communication from one binding site on F-actin to another. In this setting the initial affinity of fimbrin and F-actin would be relatively low (Fig. 5, gray actin monomers), allowing fimbrin to detach easily. This hypothesis is consistent with the observation that ABD1 decorates single filaments only partially (Hanein et al., 1997; Rost et al., 1998). However, the presence of the first bound monomer may increase the affinity of the opposite F-actin–binding site (Fig. 5 B, yellow), increasing the probability of binding a second fimbrin molecule at that site. Binding of the second fimbrin molecule is then in turn sensed by the first binding site (Fig. 5 C, now also yellow), lowering the likelihood of detachment for the first-bound fimbrin molecule, i.e., increasing its affinity to actin. The next actin filament, sharing the same polarity with the first fimbrin-bound filament, can contact the bound fimbrin only in relatively fixed geometry due to limited cross-

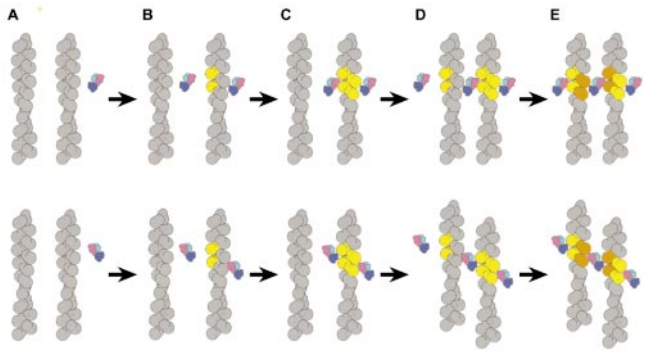

Figure 5. Possible assembly mechanism of actin–fimbrin arrays. Whether a straight or a slanted crossband appearance occurs depends on which ABD binds first to F-actin (top and bottom). ABD1 of fimbrin is pink; ABD2, blue; and the calcium-binding domain, cyan (with color scheme as described in the legend to Fig. 3). The affinity of the actin-binding sites is color coded in the following manner: gray denotes low affinity; yellow, somewhat higher affinity; and orange, the highest affinity. Note that all arguments are equally valid if ABD1 and ABD2 are exchanged within the model (e.g., ABD1 would be blue, ABD2 pink) or if the straight crossband conformation (top) is flipped 180° around the paper plane. (A) Two F-actin fragments and one unbound fimbrin molecule. (B) The fimbrin molecule is now bound to one of the F-actin fragments (with low affinity; gray), triggering higher affinity at the opposite binding site (yellow). This is presumably achieved by conformational changes in actin. A second unbound fimbrin is also shown. (C) The previously unbound fimbrin molecule is now bound to the binding site with higher affinity, triggering now higher affinity at the original first binding site (now also in yellow). (D) The second previously unbound F-actin fragment is now bound to the second fimbrin molecule with low affinity. This can only happen in a relatively fixed geometry due to the limited flexibility of the fimbrin molecule. The binding again triggers higher affinity at the opposite binding site of this filament (yellow). A third unbound fimbrin molecule is now shown. (E) The binding of the last unbound fimbrin to the binding site triggers higher affinity at the opposite previously occupied binding site on the same filament. The fimbrin molecule that is bound to both actin filaments may also trigger even higher affinities at the two contacted binding sites (orange).

bridge flexibility (maximum ~20°). Whether this geometry produces straight or slanted crossbands would depend on which ABD binds first to the filament: One will result in straight crossbands (Fig. 5, top), whereas the other will result in slanted crossbands (Fig. 5, bottom). The lack of mixed arrays suggests that actin senses whether ABD1 or ABD2 is bound at the opposite site, allowing only one type of ABD (the one that is not bound at the original binding site) to bind at the unoccupied binding site. That actin distinguishes between the two ABDs is supported by the relatively small sequence identity in fimbrin residues involved in actin binding, by different levels of suppression (Brower et al., 1995) for equivalent mutations in ABD1 and ABD2, and by the identification of two distinct dissociation constants for actin–fimbrin interactions in *A. thaliana* (Kovar et al., 2000).

We observe only very little fimbrin decoration of single isolated actin filaments, and these were not incorporated in the arrays. The rareness of single filament decoration suggests that affinity is higher when another filament is bound to the fimbrin at the opposite binding site. As a consequence of this hypothesis, one should be able to observe regular fimbrin decoration at the edge of intact arrays (side decoration). These actin-bound fimbrin molecules would not form crossbridges due to the absence of adjacent actin filaments. Indeed, we observed exactly that in our electron micrographs (Fig. 1 E). The fact that this side decoration is much more abundant than decoration of two opposite fimbrin molecules on single filaments indicates that the bonds on array sides are stronger than on single filaments. This is consistent with our proposal that the unoccupied binding site on actin not only senses the presence of fimbrin on the opposite site but also whether this fimbrin is bound to a second actin or not. The extension of this proposed mechanism into three dimensions may provide the necessary specificity for precise organization of the bundles in vivo.

3D Actin–Fimbrin Bundles

We built a 3D atomic model of actin–fimbrin bundles using the atomic model of the 2D cross-link and the bonding rules. In summary, three aspects of the bonding rules can be deduced from the data and the modeling. One, ABD1 and ABD2 bind a similar interface on actin. Two, the flexibility within the actin cross-linker complex, through the offset between allowed binding sites, is at least 20°. On the other side this flexibility needs to be <26.66°, as we do not observe slanted crossbands while filaments are in register. Three, the lack of mixed arrays and the regularity of the crossband patterns suggest that only different fimbrin ABDs (e.g., ABD1 and ABD2) can bind to the two opposite sides of the filament (not ABD1 and ABD1 or ABD2 and ABD2).

In vivo, actin–fimbrin bundles such as in the stereocilium from the hair cells of bird cochlea were shown to be organized in a hexagonal lattice, to be unipolar, and to have their filaments in register (DeRosier and Tilney, 1982). This geometry indicates that the geometry of slanted arrays (neighboring filaments not in register) does not appear in vivo. Three regularly spaced crossbands per crossover are visible in the stereocilia. Is this information consistent with our model? The three crossbands observed in these stereocilium bundles indicate that each neighboring filament in the hexagonal lattice is crossbridged once per crossover (Fig. 6 A). Starting at actin monomer 0 (located near the red crossbridge in Fig. 6 A) as the reference and using our cross-linking rules, the next crossbridge would be possible at the fourth monomer (located near the green crossbridge in Fig. 6 A) with a 6.66° counter clockwise offset from the reference position. The next crossbridge would occur at the ninth monomer with the reference geometry, but pointing in a different direction (near the blue crossbridge in Fig. 6 A). A crossbridge could then occur at the next crossover point at monomer 13 (cross-linking the same filaments as at actin monomer 0, similar to the straight 2D array) with a 6.66° counter clockwise offset from the reference position. The next crossbridge would occur at monomer 18, again with the geometry of actin monomer 0, but with reversed direction from the crossbridge at monomer 4 (compare 4 with 18 in Fig. 6, C and D). The following crossbridge at monomer 22 is offset 6.66° counter clockwise from the reference posi-

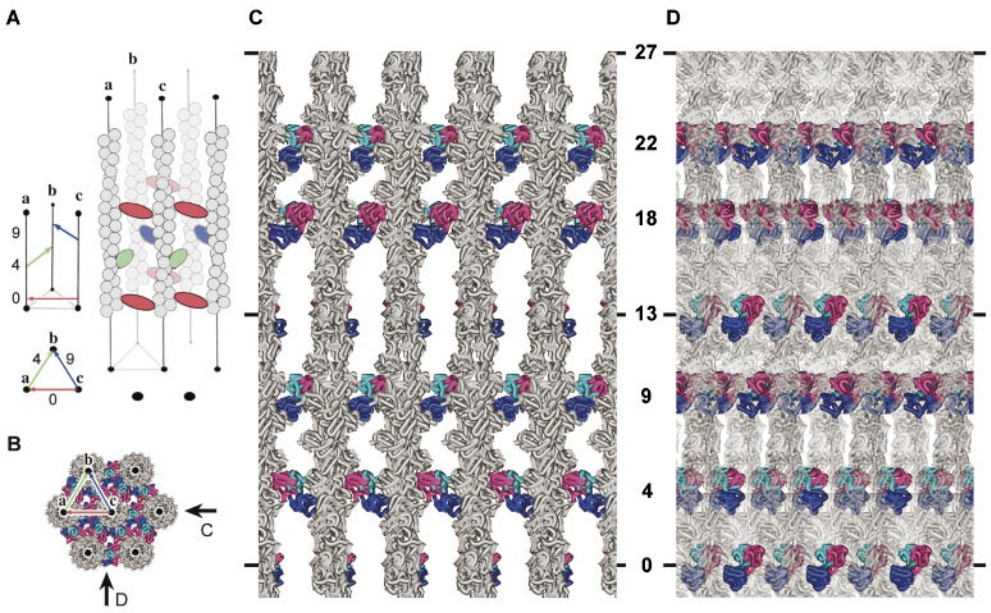

Figure 6. 3D Atomic model of an actin–fimbrin bundle. The color code is as described in the legend to Fig. 3. (A) Schematic presentation of the spatial organization of 3D actin bundles, the hexagonal lattice. (right) The gray spheres symbolize individual actin monomers, and the colored ellipses symbolize cross-linkers. (left) Further simplified schematic. Cross-linkers are symbolized by arrows, colors matching with the right side. The numbers relate to the actin monomer to which the cross-linker is bound. The triangle at the bottom is a top view of the same schematic. (B) Top view of the hexagonal lattice similar to the one that would appear in a bundle cross-section. This corresponds to a view along the [0, 0, 1] axis of the hexagonal lattice. The top view of the schematic shown in A is overlaid. The arrow labeled C shows the direction of the [1, 0, 0] axis of the hexagonal lattice, along the red arrow in A. A view along this axis is depicted in C. The arrow labeled D corresponds to the direction of the [1, 1, 0] axis of the hexagonal lattice, the view also shown in A and D. (C) Side view along the [1, 0, 0] axis of the hexagonal lattice (viewing the bundle along the red arrow in A) of the modeled actin–fimbrin bundle. This view shows the characteristic two crossbands often observed in longitudinal cross-sections in various hexagonally packed in vitro actin bundles including actin–fimbrin bundles in the stereocilia from hair cells of bird cochlea. In this view, the third crossband, corresponding to the red arrows or ellipses in A, is hidden since it is parallel to the view direction (see arrow labeled C in B). The projected spacing between the filaments corresponds to $d\sqrt{3}/2$, where d is the actual spacing (~120 Å). (D) Side view along the [1, 1, 0] axis of the hexagonal lattice (viewing the bundle when the red crossbridge in A is facing you) of the modeled actin–fimbrin bundle. The projected spacing between the filaments corresponds to d 1/2, where d is the actual spacing (~120 Å). This view shows the characteristic three crossbands as observed in longitudinal cross-sections of in vitro actin bundles. The alternating pattern of 4 and 5 monomers in between the crossbridges has also been observed in bundles (Spudich and Amos, 1979).

tion at monomer 9. The next crossbridge at monomer 27 would again be in reference geometry, but with reversed direction from the very first crossbridge at monomer 0. The emerging pattern is an alternation between one crossbridge every 4 and every 5 monomers with 6.66° offset between them, a deviation that can be easily achieved by the variability in the actin twist (~6° root-mean-square deviation) alone. The rest of the cross-link's flexibility, which can accommodate ~20° offset in total, is then still available for accommodating the necessary bending and flexibility required from these mechanoelectrical signal transducer bundles. The mechanical deformation of the hair cells is required for the depolarization and subsequent neurotransmitter release at the synapses. In situ observations show that the crossbridges tilt in respect to the filament axis when stereocilia bend (Tilney et al., 1983), indicating that the main source of flexibility is deformation of the cross-links. This flexibility of the cross-links is most likely due to the variable twist of the actin filaments actin and rearrangements at ABD1-ABD2 interface.

Structural characterization of 2D actin and actin–fimbrin arrays obtained by electron microscopy and image analysis, combined with information derived from x-ray crystallography and homology modeling, allowed us to build the first molecular model of an actin–fimbrin cross-link. Our structural model for the cross-link is in excellent agreement with the crossband patterns and interfilament spacing of stereocilia of the inner ear (DeRosier and Tilney, 1982) and of other actin bundles (DeRosier et al., 1977; Spudich and Amos, 1979; DeRosier and Censullo, 1981; Cohen et al., 1982). The data support an assembly mechanism that relies on long-range communication between the individual components of the arrays, presumably achieved by a feedback between conformational changes and changes in affinity. The regularity of the cross-linked assembly appears to be achieved through coupling between actin polymerization and cross-link formation. The model predicts the existence of flexibility within the fimbrin molecule that is consistent with a mechanism for bundle bending through tilting of the crossbridges (Tilney et al., 1983), allowing to explain how an actin bundle can be a mechanosensory machine.

We thank Dr. I. Correia for β-actin. N. Volkmann and D. Hanein thank L. Bankston for her valuable comments on the manuscript.

This work was supported by National Institutes of Health grants to D. DeRosier (GM26357) and to P. Matsudaira (CA44703). The authors acknowledge funds from the W.M. Keck Foundation.

Submitted: 10 November 2000
Revised: 11 April 2001
Accepted: 13 April 2001

References

Ayscough, K.R. 1998. In vivo functions of actin-binding proteins. *Curr. Opin. Cell Biol.* 10:102–111.

Banuelos, S., M. Saraste, and K.D. Carugo. 1998. Structural comparisons of calponin homology domains: implications for actin binding. *Structure*. 6:1419–1431.

Bartles, J.R. 2000. Parallel actin bundles and their multiple actin-bundling proteins. *Curr. Opin. Cell Biol*. 12:72–78.

Bresnick, A.R., P.A. Janmey, and J. Condeelis. 1991. Evidence that a 27-residue sequence is the actin-binding site of ABP-120. *J. Biol. Chem.* 266:12989–12993.

Brower, S.M., J.E. Honts, and A.E. Adams. 1995. Genetic analysis of the fimbrin-actin binding interaction in *Saccharomyces cerevisiae*. *Genetics.* 140:91–101.

Carugo, K.D., S. Banuelos, and M. Saraste. 1997. Crystal structure of a calponin homology domain. *Nat. Struct. Biol*. 4:175–179.

Castresana, J., and M. Saraste. 1995. Does Vav bind to F-actin through a CH domain? *FEBS Lett*. 374:149–151.

Cheng, D., J. Marner, and P.A. Rubenstein. 1999. Interaction in vivo and in vitro between the yeast fimbrin, SAC6P, and a polymerization-defective yeast actin (V266G and L267G). *J. Biol. Chem*. 274:35873–35880.

Cohen, C., B. Reinhardt, L. Castellani, P. Norton, and M. Stirewalt. 1982. Schistosome surface spines are "crystals" of actin. *J. Cell Biol*. 95:987–988.

Coluccio, L.M., and A. Bretscher. 1989. Reassociation of microvillar core proteins: making a microvillar core in vitro. *J. Cell Biol*. 108:495–502.

Corrado, K., P.L. Mills, and J.S. Chamberlain. 1994. Deletion analysis of the dystrophin-actin binding domain. *FEBS Lett*. 344:255–260.

Crowther, R.A., R. Henderson, and J. M. Smith. 1996. MRC image processing programs. *J. Struct. Biol.* 116:9–16.

de Arruda, M.V., S. Watson, C.S. Lin, J. Leavitt, and P. Matsudaira. 1990. Fimbrin is a homologue of the cytoplasmic phosphoprotein plastin and has domains homologous with calmodulin and actin gelation proteins. *J. Cell Biol*. 111:1069–1079.

DeRosier, D., and R. Censullo. 1981. Structure of F-actin needles from extracts of sea urchin oocytes. *J. Mol. Biol*. 146:77–82.

DeRosier, D.J., and L.G. Tilney. 1982. How actin filaments pack into bundles. *Cold Spring Harb. Symp. Quant. Biol*. 46:525–540.

DeRosier, D.J., and L.G. Tilney. 2000. F-actin bundles are derivatives of microvilli: what does this tell us about how bundles might form? *J. Cell Biol*. 148:1–6.

DeRosier, D., E. Mandelkow, A. Silliman, L. Tilney, and R. Kane. 1977. Structure of actin-containing filaments from two types of non-muscle cells. *J. Mol. Biol*. 113:679–695.

Egelman, E., and D. DeRosier. 1992. Image analysis shows that variations in actins crossover spacings are random, not compensatory. *Biophys. J*. 63: 1299–1305.

Fabbrizio, E., A. Bonet-Kerrache, J.J. Leger, and D. Mornet. 1993. Actin-dystrophin interface. *Biochemistry*. 32:10457–10463.

Ferrary, E., M. Cohen-Tannoudji, G. Pehau-Arnaudet, A. Lapillonne, R. Athman, T. Ruiz, L. Boulouha, F. El Marjou, A. Doye, J.J. Fontaine, et al. 1999. In vivo, villin is required for Ca^{2+}-dependent F-actin disruption in intestinal brush borders. *J. Cell Biol*. 146:819–830.

Goldsmith, S.C., N. Pokala, W. Shen, A.A. Fedorov, P. Matsudaira, and S.C. Almo. 1997. The structure of an actin-crosslinking domain from human fimbrin. *Nat. Struct. Biol*. 4:708–712.

Hanein, D., P. Matsudaira, and D.J. DeRosier. 1997. Evidence for a conformational change in actin induced by fimbrin (N375) binding. *J. Cell Biol*. 139: 387–396.

Hanein, D., N. Volkmann, S. Goldsmith, A.M. Michon, W. Lehman, R. Craig, D. DeRosier, S. Almo, and P. Matsudaira. 1998. An atomic model of fimbrin binding to F-actin and its implications for filament crosslinking and regulation. *Nat. Struct. Biol*. 5:787–792.

Holtzman, D.A., K.F. Wertman, and D.G. Drubin. 1994. Mapping actin surfaces required for functional interactions in vivo. *J. Cell Biol.* 126:423–432.

Honts, J.E., T.S. Sandrock, S.M. Brower, J.L. O'Dell, and A.E. Adams. 1994. Actin mutations that show suppression with fimbrin mutations identify a likely fimbrin-binding site on actin. *J. Cell Biol.* 126:413–422.

Keep, N.H., S.J. Winder, C.A. Moores, S. Walke, F.L. Norwood, and J. Kendrick-Jones. 1999. Crystal structure of the actin-binding region of utrophin reveals a head-to-tail dimer. *Structure Fold. Des*. 7:1539–1546.

Kovar, D.R., C.J. Staiger, E.A. Weaver, and D.W. McCurdy. 2000. AtFim1 is an actin filament-crosslinking protein from *Arabidopsis thaliana*. *Plant J*. 24: 1–14.

Kubalek, E.W., R.D. Kornberg, and S.A. Darst. 1991. Improved transfer of two-dimensional crystals from the air/water interface to specimen support grids for high-resolution analysis by electron microscopy. *Ultramicroscopy*. 35:295–304.

Lebart, M.C., C. Mejean, M. Boyer, C. Roustan, and Y. Benyamin. 1990. Localization of a new α-actinin binding site in the COOH-terminal part of actin sequence. *Biochem. Biophys. Res. Commun*. 173:120–126.

Levine, B.A., A.J. Moir, V.B. Patchell, and S.V. Perry. 1992. Binding sites involved in the interaction of actin with the N-terminal region of dystrophin. *FEBS Lett.* 298:44–48.

Lin, C.S., W. Shen, Z.P. Chen, Y.H. Tu, and P. Matsudaira. 1994. Identification of I-plastin, a human fimbrin isoform expressed in intestine and kidney. *Mol. Cell. Biol*. 14:2457–2467.

Matsudaira, P.T. 1991. Modular organization of actin crosslinking proteins. *Trends Biochem. Sci*. 16:87–92.

Matsudaira, P. 1994. The fimbrin and α-actinin footprint on actin. *J. Cell Biol.* 126:285–287.

Matsudaira, P., E. Mandelkow, W. Renner, L.K. Hesterberg, and K. Weber. 1983. Role of fimbrin and villin in determining the interfilament distances of actin bundles. *Nature*. 301:209–214.

McGough, A., M. Way, and D. DeRosier. 1994. Determination of the α-actinin–binding site on actin filaments by cryoelectron microscopy and image analysis. *J. Cell Biol.* 126:433–443.

Mimura, N., and A. Asano. 1987. Further characterization of a conserved actin-binding 27-kDa fragment of actinogelin and α-actinins and mapping of their binding sites on the actin molecule by chemical cross-linking. *J. Biol. Chem*. 262:4717–4723.

Moores, C.A., N.H. Keep, and J. Kendrick-Jones. 2000. Structure of the utrophin actin-binding domain bound to F-actin reveals binding by an induced fit mechanism. *J. Mol. Biol*. 297:465–480.

Namba, Y., M. Ito, Y. Zu, K. Shigesada, and K. Maruyama. 1992. Human T cell L-plastin bundles actin filaments in a calcium-dependent manner. *J. Biochem.* 112:503–507.

Norwood, F.L., A.J. Sutherland-Smith, N.H. Keep, and J. Kendrick-Jones. 2000. The structure of the N-terminal actin-binding domain of human dystrophin and how mutations in this domain may cause Duchenne or Becker muscular dystrophy. *Structure Fold. Des*. 8:481–491.

Orlova, A., and E.H. Egelman. 2000. F-actin retains a memory of angular order. *Biophys. J*. 78:2180–2185.

Owen, C.H., D.G. Morgan, and D.J. DeRosier. 1996. Image analysis of helical objects: the Brandeis helical package. *J. Struct. Biol*. 116:167–175.

Pearson, W.R. 1990. Rapid and sensitive sequence comparison with FASTP and FASTA. *Methods Enzymol*. 183:63–98.

Pinson, K.I., L. Dunbar, L. Samuelson, and D.L. Gumucio. 1998. Targeted disruption of the mouse villin gene does not impair the morphogenesis of microvilli. *Dev. Dyn*. 211:109–121.

Puius, Y.A., N.M. Mahoney, and S.C. Almo. 1998. The modular structure of actin-regulatory proteins. *Curr. Opin. Cell Biol*. 10:23–34.

Rost, L.E., D. Hanein, and D.J. DeRosier. 1998. Reconstruction of symmetry deviations: a procedure to analyze partially decorated F-actin and other incomplete structures. *Ultramicroscopy*. 72:187–197.

Rozycki, M., C.E. Schutt, and U. Lindberg. 1991. Affinity chromatography-based purification of profilin:actin. *Methods Enzymol*. 196:100–118.

Sali, A., and T.L. Blundell. 1993. Comparative protein modelling by satisfaction of spatial restraints. *J. Mol. Biol*. 234:779–815.

Smith, J.M. 1999. Ximdisp—a visualization tool to aid structure determination from electron microscope images. *J. Struct. Biol*. 125:223–228.

Spudich, J., and L. Amos. 1979. Structure of actin filament bundles from microvilli of sea urchin eggs. *J. Mol. Biol*. 129:319–328.

Sukow, C., and D. DeRosier. 1998. How to analyze electron micrographs of rafts of actin filaments crosslinked by actin-binding proteins. *J. Mol. Biol*. 284:1039–1050.

Taylor, K.A., and D.W. Taylor. 1994. Formation of two-dimensional complexes of F-actin and crosslinking proteins on lipid monolayers: demonstration of unipolar α-actinin-F-actin crosslinking. *Biophys. J*. 67:1976–1983.

Taylor, K.A., D.W. Taylor, and F. Schachat. 2000. Isoforms of α-actinin from cardiac, smooth, and skeletal muscle form polar arrays of actin filaments. *J. Cell Biol*. 149:635–646.

Tilney, L.G., D.J. Derosier, and M.J. Mulroy. 1980. The organization of actin filaments in the stereocilia of cochlear hair cells. *J. Cell Biol*. 86:244–259.

Tilney, L.G., E.H. Egelman, D.J. DeRosier, and J.C. Saunder. 1983. Actin filaments, stereocilia, and hair cells of the bird cochlea. II. Packing of actin filaments in the stereocilia and in the cuticular plate and what happens to the organization when the stereocilia are bent. *J. Cell Biol*. 96:822–834.

Tilney, M.S., L.G. Tilney, R.E. Stephens, C. Merte, D. Drenckhahn, D.A. Cotanche, and A. Bretscher. 1989. Preliminary biochemical characterization of the stereocilia and cuticular plate of hair cells of the chick cochlea. *J. Cell Biol*. 109:1711–1723.

Tilney, L.G., M.S. Tilney, and D.J. DeRosier. 1992. Actin filaments, stereocilia, and hair cells: how cells count and measure. *Annu. Rev. Cell Biol*. 8:257–274.

Tilney, L.G., P.S. Connelly, K.A. Vranich, M.K. Shaw, and G.M. Guild. 2000. Regulation of actin filament cross-linking and bundle shape in *Drosophila* bristles. *J. Cell Biol*. 148:87–100.

Ward, R.J., J.F. Menetret, F. Pattus, and K. Leonard. 1990. Method for forming two-dimensional paracrystals of biological filaments on lipid monolayers. *J. Electron Microsc. Tech*. 14:335–341.

Yap, K.L., J.B. Ames, M.B. Swindells, and M. Ikura. 1999. Diversity of conformational states and changes within the EF-hand protein superfamily. *Proteins*. 37:499–507.